Transcriptome and Histopathological Changes in Mouse Brain Infected with *Neospora caninum*

Maki Nishimura[1], Sachi Tanaka[1]*, Fumiaki Ihara[1], Yoshikage Muroi[2], Junya Yamagishi[3], Hidefumi Furuoka[2], Yutaka Suzuki[4] & Yoshifumi Nishikawa[1]

[1]National Research Center for Protozoan Diseases, Obihiro University of Agriculture and Veterinary Medicine, Inada-cho, Obihiro, Hokkaido, Japan, [2]Department of Basic Veterinary Medicine, Obihiro University of Agriculture and Veterinary Medicine, Obihiro, Hokkaido, Japan, [3]Research Center for Zoonosis Control, Hokkaido University, North 20, West 10 Kita-ku, Sapporo 001-0020, JAPAN, [4]Department of Medical Genome Science, University of Tokyo, Room 032, Sougou Research Complex, 5-1-5 Kashiwanoha, Kashiwa, Chiba 277-8562, Japan.

Correspondence and requests for materials should be addressed to Y.N. (nisikawa@ obihiro.ac.jp)

* Current address: Sachi Tanaka, Frontier Agriscience and Technology Center, Faculty of Agriculture, Shinshu University.

Neospora caninum is a protozoan parasite that causes neurological disorders in dogs and cattle. It can cause nonsuppurative meningoencephalitis and a variety of neuronal symptoms are observed, particularly in dogs. However, the pathogenic mechanism, including the relationship between the parasite distribution and the clinical signs, is unclear. In this study, to understand the pathogenic mechanism of neosporosis, parasite distribution and lesions were assessed in the brain of mice infected with *N. caninum* (strain Nc-1). Host gene expression was also analyzed with RNA sequencing (RNA-Seq). The histopathological lesions in the frontal lobe and the medulla oblongata were significantly more severe in symptomatic mice than in asymptomatic mice, although no association between the severity of the lesions and parasite numbers was found. In infected mice, the expression of 772 mouse brain genes was upregulated. A GOstat analysis predicted that the upregulated genes were involved in the host immune response. Genes whose expression correlated positively and negatively with parasite numbers were involved in the host immune response, and neuronal morphogenesis and lipid metabolic processes, respectively. These results suggest that changes in the gene expression profile associated with neuronal functions as well as immune responses can contribute to the pathogenesis in *N. caninum*-infected animals.

N*eospora caninum* is an intracellular apicomplexan parasite that naturally infects dogs and cattle. The infectivity of *N. caninum* for humans is unknown. However, serological evidence suggests that humans are exposed to *N. caninum*[1]. Furthermore, *Neospora* DNA has been detected in experimentally infected rhesus macaques[2]. There are three infectious stages of *N. caninum*: tachyzoites, bradyzoites in tissue cysts, and sporozoites from oocysts. Dogs probably become infected via the ingestion of tissue containing bradyzoites and cattle via the ingestion of food or drink contaminated with oocysts. Although the proliferation of tachyzoites can occur in many organs, including the heart, lung, liver, and skin, neuromuscular disorder is the clinically most important in canine neosporosis[3]. In cattle, *N. caninum* is a major cause of abortion worldwide, and calves with congenital infections can show neurological signs[4,5]. Tissue cysts are predominantly formed in the central nervous systems (CNS), and *N. caninum* is thought to show tropism for the nervous system.

Neospora caninum can cause fatal diseases in dogs of all ages, although most cases of clinical neosporosis are reported in puppies, which often show characteristic pelvic limb paralysis and rigid hyperextension[3,6]. In contrast, a variety of neurological signs are observed in adult dogs, and neurological symptoms are thought to depend on the site that is parasitized within CNS[5]. The intracellular multiplication of the tachyzoites and the subsequent cell rupture trigger the development of lesions in *N. caninum*-infected tissues[7]. However, the number of parasites is not always associated with the severity of the histopathological lesions in the brain[8,9], and the mechanism of the neuronal pathogenesis of neosporosis is unclear.

Toxoplasma gondii is closely related to *N. caninum* and causes abortion and neuronal disorders in humans and animals. It has also been suggested that chronic infection with *T. gondii* can involve behavioral changes and psychiatric disorders in humans and animals[10]. In a previous study, we investigated the gene expression profiles and histopathological changes in the brains of mice infected with *T. gondii*, and our findings indicated that *T. gondii* stimulated the immune response including antigen presentation and diminished signal transduction

included small-GTPase-mediated signal transduction and vesicle formation, which both regulate neurological functions in the brain[11]. Therefore, changes in gene expression caused by *N. caninum* infection potentially contribute to the neuronal pathogenesis in *N. caninum*-infected animals.

Some strains of mice including BALB/c are susceptible to *N. caninum* and exhibit encephalitis caused by the parasite infection[12]. Therefore mice have been used widely as an infection model of neosporosis to investigate immune responses and vaccine efficacy[13]. In this study, to understand the mechanism of neuronal pathogenesis during subacute infection with *N. caninum*, we investigated the histopathological changes, the distribution of the parasite, and the gene expression profiles (using a whole-transcriptome shotgun sequencing approach, RNA-Seq) in the brains of mice infected with *N. caninum*.

Results

Mice infected with *N. caninum* showed characteristic clinical signs and histopathological changes in the brain. Pathological severity was evaluated in 17 mice, and 10 of the 17 mice showed clinical signs of neosporosis including febrile responses and leg paralysis 39 days after infection (See Figure 1A). Seven of 10 symptomatic mice showed neurological signs, including circling motion, head tilting, and leg paralysis. We analyzed the nine area of brain histopathologically and for the quantification of parasite load. Histopathological lesions, including perivascular cuff, mononuclear cellular meningitis, glial cell activation, and focal necrosis, were observed in the brains of all 17 mice, which are similar to the lesions found in dogs[8,9,14,15]. Each focal lesion was scored for severity using a scale from 1 to 4 (See Figure 2A–D). The total pathological scores for all areas in the brain are shown in Figure 2E. The total scores for the frontal lobe and medulla oblongata were significantly higher in the symptomatic mice than in the asymptomatic mice. Although there were no significant differences between the symptomatic and asymptomatic mice in the cerebellum, two symptomatic mice showed very high scores.

Tachyzoites were found within some lesions, but no tissue cysts were found in the present study. Therefore, the tropism of tissue cysts was not determined histopathologically. We also investigated the distribution of the parasite in the brain with real-time PCR. The numbers of parasites for each area of the brain are shown in Figure 2F. A sporadically high parasite load was detected in the frontal lobe and periaqueductal gray of the symptomatic mice. However we could not evaluate the difference of parasite number among the areas statistically because of small sample number. No association between the parasite load and the severity of the lesions was found. In an immunohistochemical analysis, the infiltration of macrophages or microglia and the production of inducible nitric oxide synthase (iNOS) were predominantly observed in the necrotic and inflammatory lesions (See Figure 3).

Gene expression profiles are altered in their brains of mice infected with *N. caninum*. Eight mice, consisting of four *N. caninum*-infected mice and four uninfected mice, were used in the transcriptome analysis (See Figure 1B). Two of the four *N. caninum*-infected mice showed clinical signs of neosporosis, including starry coat and hunched back, 39 days after infection. The numbers of parasites tended to be slightly higher in the symptomatic mice (See supplementary Table S1). RNA obtained from the eight mice was subjected to high-throughput sequencing on an Illumina Genome Analyzer IIx. Eight libraries were sequenced and 34–47 million raw sequence reads were obtained per sample. Of these, 63.5%–84.9% could be mapped to the mouse genome (See supplementary Table S2).

To identify the differentially expressed genes in the experimental groups, we analyzed the transcriptome data from the *N. caninum*-infected and uninfected mouse brains with DESeq. The magnitude distribution of the significantly altered genes was illustrated with an MA plot analysis (See supplementary Figure S1). We analyzed 37,306 genes including 22,661 protein-coding genes. The expression of 772 protein-coding genes (2.1% of all analyzed genes and 3.4% of protein-coding genes) in the brains of the mice infected with *N. caninum* was significantly upregulated relative to their expression in the uninfected mice. The 30 most upregulated genes after infection with *N. caninum* are listed in Table 1. These 30 genes included genes for chemokines and chemokine receptors (*Cxcl9*, *Ccl8*, *Ccl5*, *Cxcl10*, and *Cxcr6*), immunoglobulins (*Ighg2c*, *Iglc2*, and *Igj*), interferon (IFN)-inducible GTPase family members (*Tgtp2*, *Gbp8*, and *Iigp1*), and MHC class II antigens (*Cd74*, *H2-Eb1*, *H2-Aa*, and *H2-Q7*). The quantitative PCR analysis showed that expression of *Ccl8*, *Ccl5*, *Cxcl10*, *Cxcr6*, *Tgtp2*, *Gbp8*, *Iigp1* and *Saa3* were significantly upregulated in the brains of *N. caninum*-infected mice (See Figure 4). In contrast, only three genes (*Fcrls*, *Myoc*, and *Gkn3*) were significantly downregulated in the infected mice (See supplementary Table S3). When the functional annotations of the genes upregulated by *N. caninum* infection were analyzed using GOstat, gene ontology (GO) terms associated with immune system processes, immune responses, and cell activation were represented significantly more strongly in the upregulated genes compared with the reference genes (See Table 2).

Gene expression levels correlate with the numbers of parasites in the brain. To investigate whether the fragments/kb of transcripts/million fragments mapped (FPKM) value correlates with the number of parasites in the infected mouse brain, the correlation coefficients were calculated. Seven hundred and twenty-two genes correlated positively with the numbers of parasites measured, whereas 320 genes showed negative correlations. There were 253 genes overlapping between genes upregulated by infection and genes correlated positively with the number of parasites (See supplementary Table S4). Ten (*Cd8a*, *F10*, *F830016B08Rik*, *Il1rn*, *Lcn2*, *Cxcl10*, *Kirk1*, *Gimap7*, *Cxcr6* and *Irg1*) of the 30 genes most upregulated in *N. caninum* infected mice were not overlapped with the genes correlated positively with the number of parasites. Table 3 and Table 4 show the thirty most overrepresented GO terms for the genes that correlated positively and negatively with the parasites load, respectively. The GOstat analysis showed that the genes whose expression correlated positively with parasite numbers were associated with lysosome and ribosome in addition to immune responses. In contrast, the statistically overrepresented GO terms for the genes whose expression correlated negatively with parasite numbers involved cell and neuron projection, sterol and steroid metabolic processes, and synaptic transmission. These results indicate that *N. caninum* stimulates translational activation and intracellular digestion and reduce cell morphogenesis, including that of axons and dendrites, lipid metabolism, and neural transmission.

Gene expression profiles of symptomatic mice differed from those of asymptomatic animals. The severity of the clinical signs of neosporosis differed among the *N. caninum*-infected mice (See supplementary Table S1). To identify differences in the gene expression profiles associated with the development of neosporosis, the genes expressed differentially between symptomatic and asymptomatic mice were analyzed with DESeq. The expression of no gene was higher in the symptomatic mice than in the asymptomatic mice, but the expression of eight genes was lower in the symptomatic mice than in the asymptomatic mice (See Table 5). These genes encoded solute carrier family 6 (a neurotransmitter transporter, serotonin), member 4 (SLC6A4), solute carrier family 6 (a neurotransmitter transporter, glycine), member 5 (SLC6A5), tryptophan hydroxylase 2 (TPH2), and low-density lipoprotein receptor (LDLR). Although we could not evaluate
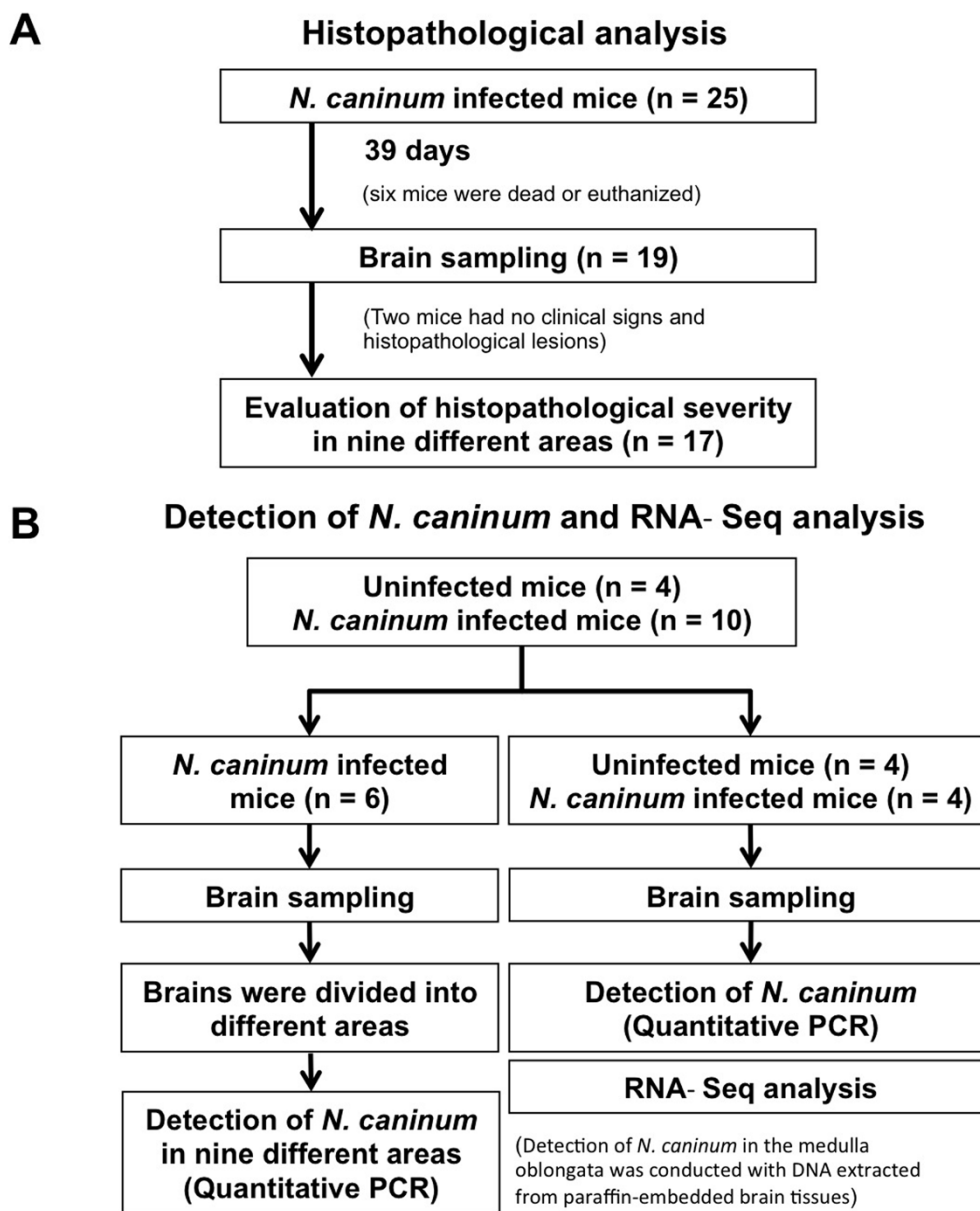
2

Figure 1 | Flow diagram illustrating the number of mice used in each analysis. (A) For the histopathological analysis, 25 mice were infected with *N. caninum*. Because eight of the 25 mice died before sampling or may not have been infected, the severity of the brain lesions in nine different areas (olfactory system, frontal lobe, caudate putamen, hippocampus, hypothalamus, amygdala, periaqueductal gray, medulla oblongata and cerebellum) was estimated in 17 mice (ten symptomatic and seven asymptomatic mice). (B) For the detection of *N. caninum* and the RNA-Seq analysis, 14 mice were used (four uninfected and 10 infected mice). Thirty-nine days after inoculation, six of the 10 infected mice showed clinical signs of neosporosis, but four animals did not. To detect *N. caninum* in different areas of the brain, six infected mice were selected (four symptomatic and two asymptomatic mice). The brains of these six infected mice were divided into eight different areas (olfactory system, frontal lobe, caudate putamen, hippocampus, hypothalamus, amygdala, periaqueductal gray, and cerebellum), and used for DNA extraction and quantitative PCR analysis of the parasite. Additionally, to detect *N. caninum* in the medulla oblongata, DNA was extracted from paraffin-embedded brain tissues containing the medulla oblongata and cerebellum (n = 17, from mice shown in Figure 1A) and subjected to quantitative PCR. For the detection of *N. caninum* in whole-brain samples and the RNA-Seq analysis, four uninfected and four infected (two symptomatic and two asymptomatic mice) brains were used. DNA and RNA were extracted from each brain sample and used for the quantitative PCR analysis of the parasite numbers and the RNA-Seq analysis.

the difference of gene expression between symptomatic and asymptomatic mice statistically because of small sample number, *Slc6a4, slc6a5, Tph2 and ldlr* tended to be downredulated in symptomatic mice in quantitative PCR analysis (See Figure 4).

Discussion

The BALB/c mouse is known to be susceptible to the development of encephalitis induced by *N. caninum* and encephalitis is observed several weeks after inoculation[12,16]. In a previous study of *T. gon-* *dii*-infected mouse brains, we showed that the frontal lobe was more affected than any other area of the brain, whereas tissue damage and parasite infection were minor in the cerebellum[11]. The frontal lobe and medulla oblongata were mainly affected in symptomatic mice infected with *N. caninum* and some mice showed severe histopathological lesions in the cerebellum. Therefore, lesion formation in the medulla oblongata and the cerebellum may be characteristic of *N. caninum* infection. These results suggest that damage to neuronal tissues in the frontal lobe, medulla oblongata, and cerebellum is
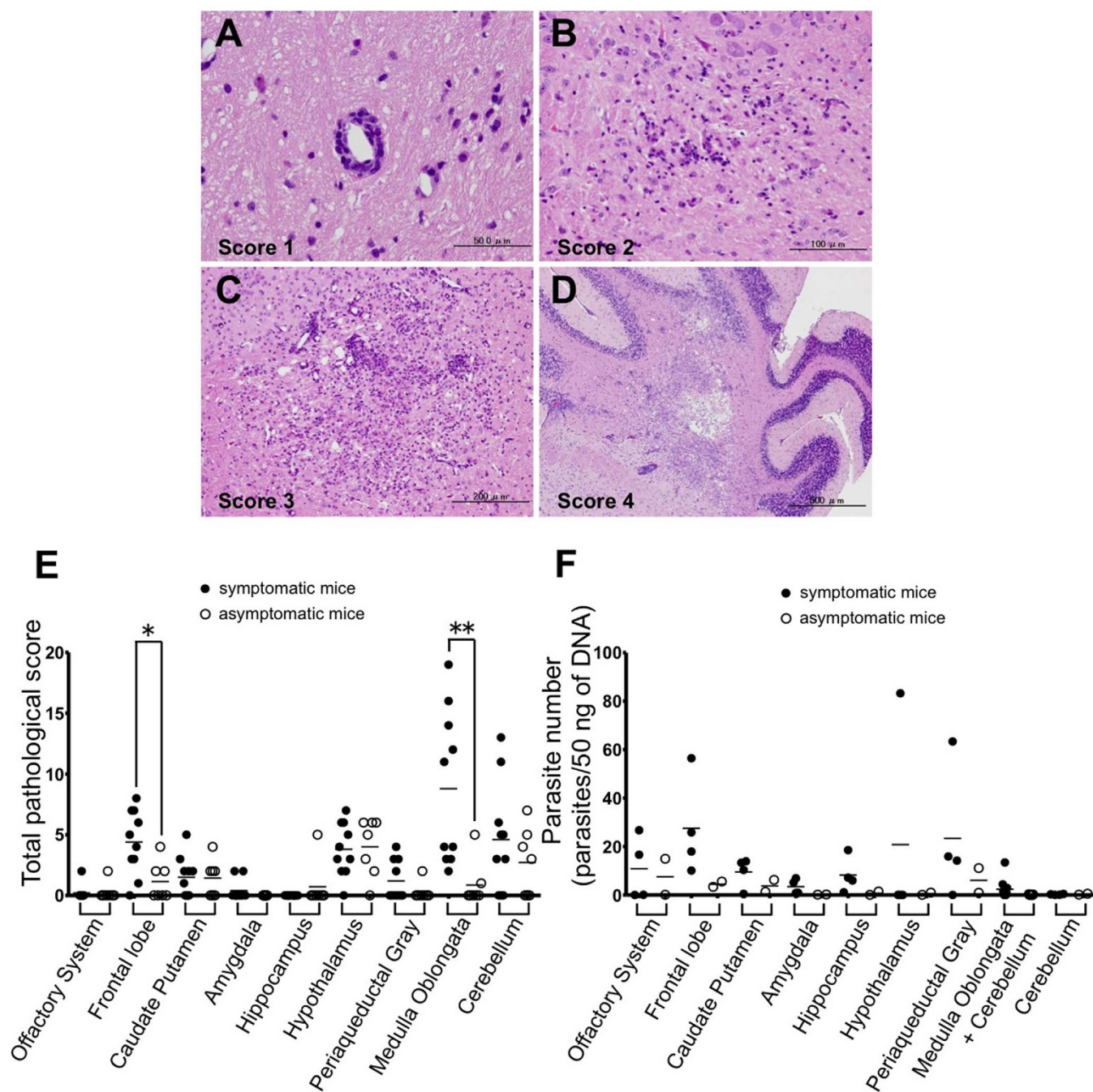
Figure 2 | Histopathological lesions and parasite distributions in different areas of *N. caninum*-infected mouse brains. (A–D) Histopathological lesions in mouse brains infected with *N. caninum* (n = 17). To estimate the severity of the histopathological lesions, the lesions were scored as follows: (A) localized perivascular cuff (score 1), (B) local gliosis (score 2), (C) focal necrosis with moderate inflammatory cell infiltration (score 3), and (D) severe glial cell and macrophage infiltration, and rarefaction of the neuropil in extensive necrotic foci (score 4). (E) The total pathological scores for different mouse brain areas were determined as described in the Materials and Methods (ten symptomatic and seven asymptomatic mice). *p < 0.05 and **p < 0.01 (unpaired Student's *t*-test). (F) After DNA extraction from *N. caninum*-infected mouse brain samples (four symptomatic and two asymptomatic mice) and paraffin-embedded brain tissues, including the medulla oblongata and cerebellum (ten symptomatic and seven asymptomatic mice), parasite numbers were quantified by real-time PCR using primers specific for the *N. caninum* Nc5 gene.

associated with the pathogenesis of neosporosis. Some infectious diseases including listeriosis show brain stem tropism[17]. *Listeria monocytogens*, which is enable to survive and multiply in macrophages, invades in the brain by centripetal migration along cranial nerve[17] and interaction between infected myeloid cell and endothelium[18]. *T. gondii* and *N. caninum* are thought to be delivered to organs by infected leukocytes in the blood. Although no association between the severity of the lesions and parasite numbers was found, endothelium in brain stem may be prone to adhere to pathogen-infected leukocyte and obstruction by

leukocyte adhesion may lead to the damage of parenchyma of brain. Expression of adhesion molecule in each area of brain is intriguing. In some adult cases of canine neosporosis, the cerebellum and brainstem are predominantly affected[8,14,15]. Those cases suggest that the cerebellum can be the most commonly affected region in adult dogs with neosporosis[14]. Therefore, the murine model of neosporosis could be help clarifying the pathology in adult dogs.

In this study, no association between the parasite load and the severity of the lesions in each area was found. In canine neosporosis,
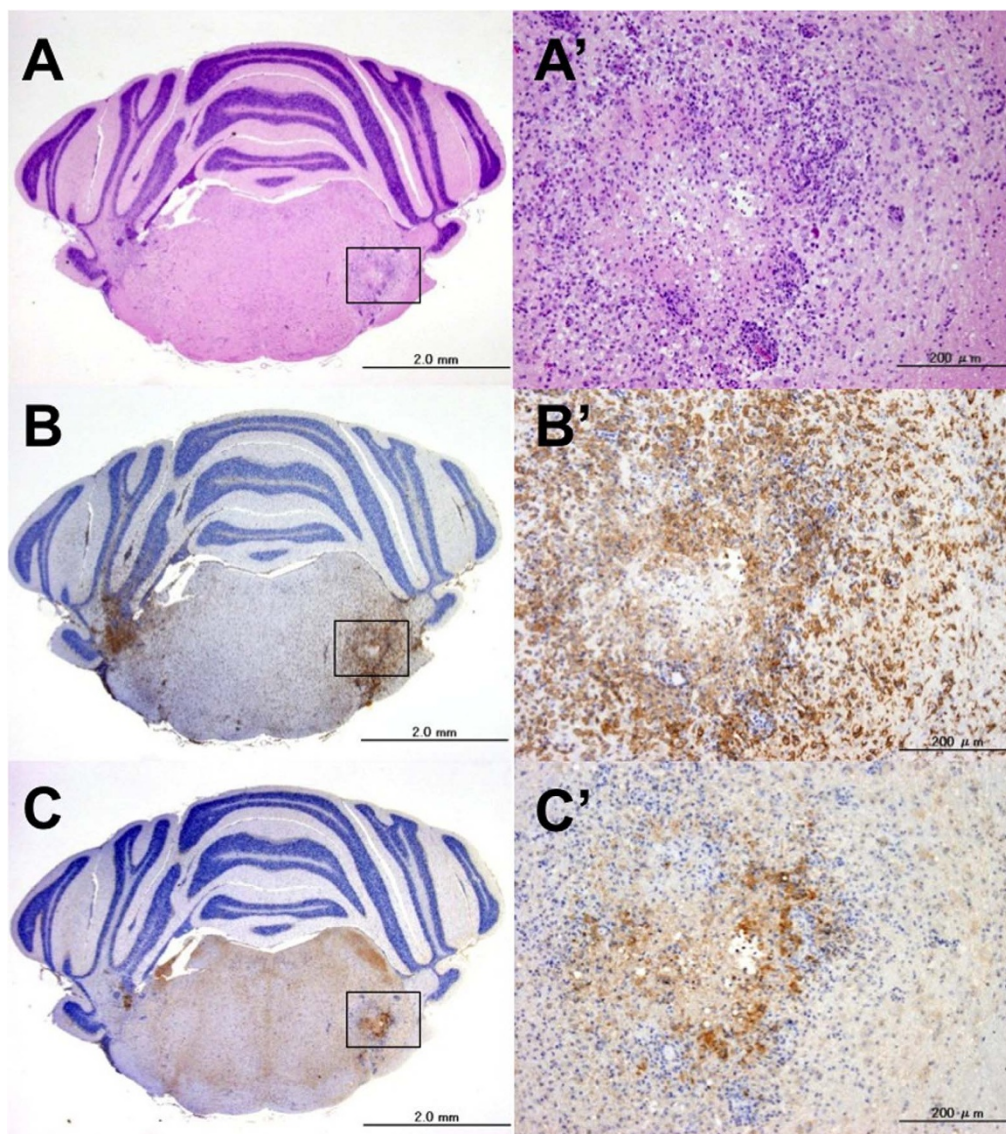
Figure 3 | Immunohistochemical analysis of macrophages/microglia and iNOS in lesions of *N. caninum*-infected mouse brain. (A–C) Serial sections of *N. caninum*-infected mouse brain. (A and A′) HE staining. (A′) A high-magnification image showing focal necrosis with mononuclear cell infiltration and cuffing. (B and B′) Immunohistochemical analysis with anti-Iba1 antibody. Infiltration of activated macrophages/microglia was observed around the necrotic area. (C and C′) Immunohistochemical analysis with an anti-iNOS antibody. Expression of iNOS was detected in inflammatory cells around the necrotic areas.

a disassociation between parasite density and the severity of tissue damage has also been reported in adult cases[8,9]. Therefore, host factors, which can cause or exacerbate tissue damage, may be involved in the pathogenesis of neosporosis. In the brains of *N. caninum* infected mice, infiltration of macrophages or microglia and the production of iNOS were observed in the lesions. Activated microglia and astrocyte produce neurotoxic factors including nitric oxide (NO). NO produced by activated microglia and astrocytes inhibits neuronal respiration and causes glutamate release from neurons, which results in neuronal death from glutamate excitotoxicity via the N-methyl d-aspartate (NMDA) receptor[19,20]. Therefore, NO may be a factor that exacerbates brain tissue damage in neosporosis.

The 30 genes most strongly upregulated by *N. caninum* infection were similar to those upregulated in *T. gondii*-infected mice[11]. IFN-inducible GTPases play an important role in the host defense against intracellular pathogens, including *T. gondii*[21]. IIGP1 (IRGA6: immunity–related GTPase family member a6) is a member of the p47 GTPase family, and the accumulation of IIGP1 on the parasitophorous vacuole membrane of *T. gondii* resulted in the disruption of

the membrane[22,23] and the necrotic death of the infected cell[23]. We showed that *Iigp1* was significantly upregulated in the brain of *T. gondii* infected mice in previous study[11]. ROP18 is a rhoptry kinase expressed highly by virulent *T. gondii* and phosphorylates and inactivates immunity-related GTPase (IRGs). However, genome sequencing and transcriptome analysis of *N. caninum* Liverpool strain revealed that *ROP18* in *N. caninu* is a pseudogene and *N. caninum* is unable to prevent the host from using IRGs to disrupt the parasitophorous vacuole[24]. This suggests that the growth of *N. caninum* could be inhibited effectively, which can lead to low parasite number in the lesions. A previous study showed that CXCL9/MIG, CXCL10/IP-10, and CCL5/RANTES are induced, dependent on IFN-γ, in the brains of BALB/c mice during chronic infection with *T. gondii*[25]. Protective immunity against *N. caninum* involves the Th1-type immune response, including IFN-γ and interleukin 12 (IL-12) production[16,26], and CCL5 induces the migration of Th1 cells via chemokine receptors including CCR5[27]. On the other hand, some studies have indicated that chemokines and their receptors are involved in exacerbating neuronal damage. Ischemic brain injury was exacer-

Table 1 | Thirty genes most significantly upregulated in *N. caninum*-infected mouse brains

Gene symbol	Description	Average of FPMK		Fold change	FDR
		Uninfected (n = 4)	Infected (n = 4)		
Saa3	serum amyloid A 3	0.12	258.01	1989.26	3.33E-05
Cxcl9	chemokine (C-X-C motif) ligand 9	0.01	19.27	1581.14	1.83E-07
Ighg2c	immunoglobulin heavy constant gamma 2C	0.34	401.45	1196.80	1.53E-12
Ccl8	chemokine (C–C motif) ligand 8	0.08	88.64	1065.20	3.29E-04
Cd8a	CD8 antigen, alpha chain	0.00	3.03	1029.22	6.60E-08
F10	coagulation factor X	0.01	5.48	952.87	4.34E-06
F830016B08Rik	RIKEN cDNA F830016B08 gene	0.00	2.52	917.74	1.30E-11
Iglc2	immunoglobulin lambda constant 2	0.02	14.02	694.68	3.94E-07
Ccl5	chemokine (C–C motif) ligand 5	0.38	231.64	611.07	3.11E-05
Il1rn	interleukin 1 receptor antagonist	0.02	2.55	535.78	1.83E-06
Tgtp2	T cell specific GTPase 2	0.10	13.67	533.21	1.08E-11
Lcn2	lipocalin 2	0.09	41.88	512.67	1.22E-09
Nkg7	natural killer cell group 7 sequence	0.01	6.24	494.87	3.94E-07
Cd74	CD74 antigen (invariant polypeptide of major histocompatibility complex, class II antigen-associated)	2.57	1281.31	484.61	6.26E-10
Gm4951	predicted gene 4951	0.81	355.49	484.61	7.30E-10
H2-Eb1	histocompatibility 2, class II antigen E beta	0.77	217.08	461.83	5.20E-09
Igj	immunoglobulin joining chain	0.03	11.31	450.15	7.14E-06
Gbp8	guanylate-binding protein 8	0.05	20.43	389.61	2.04E-05
Cst7	cystatin F (leukocystatin)	0.17	43.87	387.41	1.78E-04
Cxcl10	chemokine (C-X-C motif) ligand 10	1.60	530.34	378.75	1.51E-06
H2-Aa	histocompatibility 2, class II antigen A, alpha	0.17	57.55	351.69	2.33E-10
Iigp1	interferon inducible GTPase 1	0.06	29.46	339.64	1.25E-08
Zbp1	Z-DNA binding protein 1	0.01	1.94	334.68	2.61E-09
Klrk1	killer cell lectin-like receptor subfamily K, member 1	0.05	15.91	329.33	9.59E-05
H2-Q7	histocompatibility 2, Q region locus 7	0.01	2.32	324.26	5.60E-12
Gimap7	GTPase, IMAP family member 7	0.02	6.33	305.31	2.17E-04
Apoc2	apolipoprotein C-II	0.01	2.63	303.69	1.64E-07
Cxcr6	chemokine (C-X-C motif) receptor 6	0.10	22.60	295.81	1.30E-05
Fcgr4	Fc receptor, IgG, low affinity IV	0.01	3.15	265.63	1.11E-04
Irg1	immunoresponsive gene 1	0.81	355.49	241.83	1.57E-05

(>two-fold change and FDR < 0.05)

bated by a systemic increase in CCL5 during a Th1-polarized response induced by infection[28] and the downregulation of CCR5 protected the brain from neuron loss, inflammation, and seizure activity[29]. Therefore, the chemokines upregulated by *N. caninum* infection may be involved in both protective immunity and neuronal pathogenesis. *Saa3* expression was also highly upregulated in the mouse brain after *N. caninum* infection. Serum amyloid A (SAA) is an acute-phase protein, and a previous study suggested that SAA3 activates Toll-like receptor 2 (TLR2) and TLR4 as an endogenous ligand in astrocytes infected with herpes simplex virus type 1[30]. SAA3 is also produced in Schwann cells and macrophages in injured peripheral nerves[31]. Thus, SAA3 may act as a cytokine and be involved in the immune response and neuronal degeneration.

Only three genes (*Fcrls*, *Myoc*, and *Gkn3*) were significantly downregulated in the infected mice. *Myoc* is related to myelination in the peripheral nerve[32] and *Fcrls* was previously known as macrophage scavenger receptor 2 (*Msr2*) and is upregulated by mild traumatic brain injury[33], and downregulated in brain infected *T. gondii*[11] and Japanese encephalitis virus[34]. Although function of *Fcrls* is not well known in brain, downregulation of *Fcrls* is thought to be associated with host-pathogen interaction.

The GOstat analysis showed that the genes whose expression correlated negatively with parasite numbers involved cell and neuron projection, sterol and steroid metabolic processes, and synaptic transmission. Cholesterol is a component of cell membranes, and neurons and astrocytes demand high levels of cholesterol because they have the enormous membrane surfaces, encompassing their axons, dendrites, synapses, and processes[35]. Cholesterol is also

required for cell regeneration after CNS injury and for the formation of new synapses. Cholesterol levels can also affect the biophysical function of membranes, and changes in cholesterol levels of membrane have been shown to affect the excitability of rat hippocampal neurons[36]. Therefore, changes in the expression of genes that are involved in cellular morphogenesis and lipid metabolism, including cholesterol, may be involved in the exacerbation of neuronal damage, impaired regeneration of damaged neuronal tissues, and the disruption of neurotransmission in mouse brains infected with *N. caninum*.

The expression of eight genes including *Hoxb5*, *Slc6a4*, *Slc6a5*, *Tph2* and *Ldlr* was lower in the symptomatic mice than in the asymptomatic mice. *Hoxb5* is a gene of gene family cording for transcription factors and Hoxb5 protein is expressed in mice lung during development[37]. A previous study demonstrated that mice deficient in glycine transporter 2 encoded by *Slc6a5* showed neuromotor abnormalities, such as spasticity, hind feet clasping, and tremor[38]. Tryptophan hydroxylase 2 encoded by *Tph2* is the key enzyme in brain serotonin synthesis[39], and it is possible that serotonergic neurons work poorly in mice that develop neosporosis. Therefore, the reduced expression of genes for neurotransmitter transporters may contribute to the development of neosporosis by modulating serotonergic and glycinergic neurotransmission.

In this study, we demonstrated that the frontal lobe and medulla oblongata were most often affected in *N. caninum*-infected mice with clinical signs and that there was no association between the parasite load and the severity of the histopathological lesions. Changes in the gene expression profile were also observed in the mouse brains after *N. caninum* infection. Genes associated with the immune response,
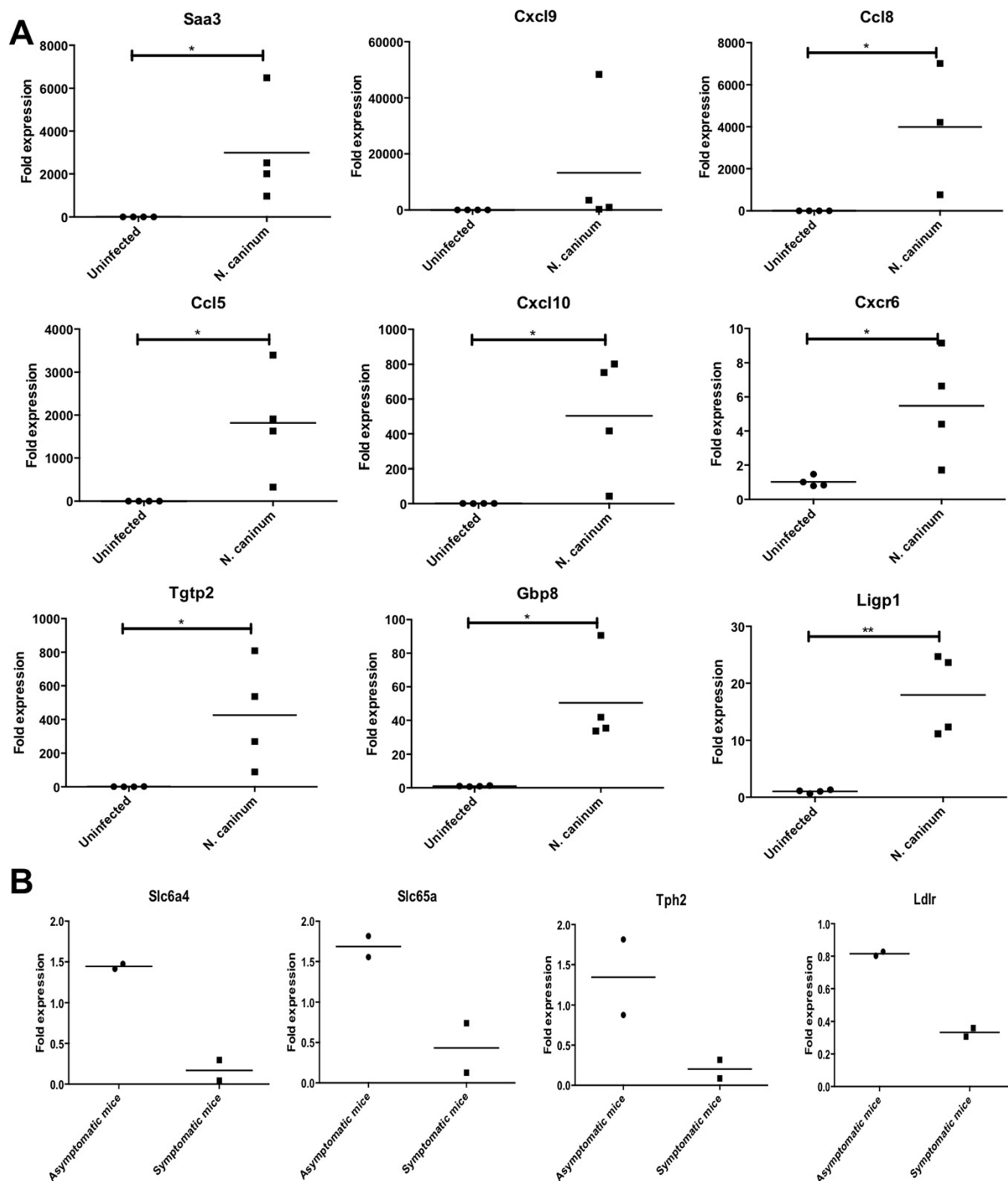
Figure 4 | Gene expression analysis by quantitative PCR using RNA from the brain samples used in RNA-seq analysis. (A) Expression of the genes (*Saa3*, *Cxcl9*, *Ccl8*, *Ccl5*, *Cxcl10*, *Cxcr6*, *Tgtp2*, *Gbp8* and *Ligp1*) that upregulated by *N. caminum* infection. (B) Expression of the genes (*Slc6a4*, *Slc6a5*, *Tph2* and *Ldlr*) that downregulated in symptomatic mice infected with *N. caninum*. *$p < 0.05$ and **$p < 0.01$.

encoding chemokines and IFN-inducible GTPase family members, were upregulated in the brains of mice infected with *N. caninum*. In contrast, the expression of genes associated with the morphogenesis of neurons, including their synapses and projections, with lipid metabolism, and with neuronal transmission correlated negatively with the number of parasites. These results suggest that neuronal tissue damage is caused by the inflammatory responses to parasite infection and can be exacerbated by the impairment of the regeneration of damaged neuronal tissue. Our results also suggest that neuronal transmission is affected by *N. caninum* infection at the level of

Table 2 | GO terms for the most significantly upregulated genes in mouse brains after infection with *N. caninum*

Accession	GO term	Reference genes		Up-regulated genes		FDR
		# Genes	%	# Genes	%	
GO:0002376	immune system process	566	3.8	184	28.4	0
GO:0006952	defense response	353	2.4	104	16.0	0
GO:0006955	immune response	346	2.3	138	21.3	0
GO:0006954	inflammatory response	178	1.2	64	9.9	5.92E-64
GO:0009897	external side of plasma membrane	121	0.8	51	7.9	6.28E-59
GO:0009986	cell surface	168	1.1	58	8.9	2.06E-55
GO:0045321	leukocyte activation	189	1.3	60	9.2	1.41E-52
GO:0001775	cell activation	202	1.4	62	9.6	1.64E-52
GO:0009611	response to wounding	252	1.7	69	10.6	1.10E-51
GO:0002682	regulation of immune system process	92	0.6	41	6.3	1.50E-49
GO:0050776	regulation of immune response	90	0.6	40	6.2	3.46E-48
GO:0051239	regulation of multicellular organismal process	250	1.7	65	10.0	1.01E-45
GO:0009605	response to external stimulus	393	2.6	83	12.8	1.57E-45
GO:0046649	lymphocyte activation	173	1.2	53	8.2	1.36E-44
GO:0042110	T cell activation	112	0.7	39	6.0	5.58E-37
GO:0002252	immune effector process	113	0.8	38	5.9	1.10E-34
GO:0051240	positive regulation of multicellular organismal process	96	0.6	34	5.2	1.51E-32
GO:0001816	cytokine production	95	0.6	33	5.1	6.63E-31
GO:0002520	immune system development	228	1.5	49	7.6	1.39E-26
GO:0006935	chemotaxis	92	0.6	30	4.6	4.22E-26
GO:0042330	taxis	92	0.6	30	4.6	4.22E-26
GO:0048534	hemopoietic or lymphoid organ development	212	1.4	45	6.9	6.89E-24
GO:0019882	antigen processing and presentation	43	0.3	33	5.1	2.91E-23
GO:0006950	response to stress	666	4.5	87	13.4	2.07E-22
GO:0030097	hemopoiesis	190	1.3	40	6.2	8.01E-21
GO:0005886	plasma membrane	1476	9.9	143	22.0	1.76E-20
GO:0051249	regulation of lymphocyte activation	76	0.5	36	5.5	3.31E-20
GO:0050865	regulation of cell activation	79	0.5	36	5.5	8.86E-20
GO:0048002	antigen processing and presentation of peptide antigen	28	0.2	26	4.0	1.33E-19
GO:0002521	leukocyte differentiation	118	0.8	30	4.6	1.33E-19

gene transcription, and that neurological symptoms can be induced not only by organic damage but also by neuronal dysfunction.

Methods

Ethics Statement. This study was performed in strict accordance with the recommendations in the Guide for the Care and Use of Laboratory Animals of Ministry of Education, Culture, Sports, Science and Technology, Japan. The protocol was approved by the Committee on the Ethics of Animal Experiments of the Obihiro University of Agriculture and Veterinary Medicine (Permit number 25–59, 25–60, 25–62). All surgery was performed under isoflurane anesthesia, and all efforts were made to minimize animal suffering.

Mice. Mice used in this study were treated and used according to the Guiding Principles for the Care and Use of Research Animals published by the Obihiro University of Agriculture and Veterinary Medicine. Female BALB/c mice were obtained from CLEA Japan (Tokyo, Japan). The mice were housed under specific-pathogen-free conditions in the animal facility of the National Research Center for Protozoan Diseases at the Obihiro University of Agriculture and Veterinary Medicine, Obihiro, Japan, before they were used in the experiments at 8 weeks of age.

Preparation of *N. caninum* tachyzoites and parasite infection of mice. *Neospora caninum* tachyzoites of strain Nc-1[40] were propagated in monkey kidney adherent fibroblasts (Vero cells) cultured in Eagle's minimum essential medium (Sigma, St. Louis, MO, USA) supplemented with 8% heat-inactivated fetal bovine serum. For the purification of the tachyzoites, the parasites and host-cell debris were washed in cold phosphate-buffered saline (PBS), and the final pellet was resuspended in cold PBS and passed through a 27-gauge needle and a 5.0-μm pore filter (Millipore, Bedford, MA, USA). Eight-week-old mice were inoculated intraperitoneally with *N. caninum* parasites purified from an *in vitro* culture. All the mice were checked regularly for clinical signs of *N. caninum* infection, such as febrile responses (e.g., a starry stiff coat), hunched back, and limb paralysis.

Brain sampling. For the histopathological analysis, 25 mice were infected with 1×10^6 *N. caninum*. Because six mice died or were euthanized before the scheduled date as a result of emaciation, 19 mice were sampled. Thirty-nine days after inoculation, at which time histopathological changes have occurred, the experimental mice were killed and their brains rapidly removed (See Figure 1). The brains were fixed with a 10% neutral-buffered formalin solution for 6 days. We used these brains in the

histopathological and immunohistochemical analyses. Two of 19 mice showed no clinical symptoms and no pathological changes. Because it was possible that the parasite had not infected these two mice, the distribution and severity of the brain lesions were estimated in the remaining 17 of 19 mice. Of the 17 mice, 10 mice showed clinical signs of neosporosis 39 days after infection (See Figure 1).

Fourteen mice (four uninfected mice and 10 infected mice) were used for the detection of *N. caninum* and the RNA-Seq analysis (See Figure 1). Thirty-nine days after infection, six infected mice showed the clinical signs of neosporosis and four animals did not. To detect *N. caninum* in different areas of the brain, six infected mice were selected (four symptomatic and two asymptomatic mice). The brains of these six infected mice were divided into eight different areas, the olfactory system, frontal lobe, caudate putamen, hippocampus, hypothalamus, amygdala, periaqueductal gray, and cerebellum. The samples to be used for DNA extraction and quantitative PCR of the parasites were stored at $-20°C$ until analysis.

We used the other eight mice (four uninfected and four infected mice) to detect *N. caninum* in whole brain samples and in the RNA-Seq analysis. Of the four infected mice, two were symptomatic and two were asymptomatic. The brains of four infected mice and four uninfected mice were individually homogenized in 1 mL of TRI Reagent (Sigma-Aldrich, Tokyo, Japan). Each brain sample was then divided for DNA extraction (for quantitative PCR of the parasite numbers) or RNA extraction (for the RNA-Seq analysis).

Pathological analysis. After fixation, the brain samples were cut coronally, embedded in paraffin wax, sectioned to 4 μm, and then stained with hematoxylin and eosin (HE). To estimate the severity of the histopathological lesions, they were scored with the following scheme: 0, no lesion; 1, minimal lesions limited to localized perivascular cuffs or slight mononuclear cell infiltration in the meninges; 2, mild lesions, including perivascular cuffs, meningitis, and local glial cell infiltration; 3, moderate lesions, including perivascular cuff, meningitis, glial cell activation, focal necrosis, and rarefaction of the neuropil, with occasional macrophage infiltration; 4, severe lesions, including perivascular cuffs, meningitis, glial cell activation, rarefaction of the neuropil, and extensive necrosis. The severity of the brain lesions was estimated in nine different areas including olfactory system, frontal lobe, caudate putamen, hippocampus, hypothalamus, amygdala, periaqueductal gray, medulla oblongata and cerebellum. The scores for each lesion were added for each area, and the total pathological score for each area was used in the data analysis. Pathological lesions representing the different scores are shown in Figure 2A–D. Statistical significance of the differences between symptomatic and asymptomatic mice was investigated by t test. $P < 0.05$ was considered statistically significant.

Table 3 | Thirty most overrepresented GO terms for the genes that correlated positively with the parasites load

Accession	GO term	Reference gene		Genes positively correlated with parasite number		FDR
		# Genes	%	# Genes	%	
GO:0002376	immune system process	566	3.8	93	15.0	1.29E-37
GO:0006955	immune response	346	2.3	65	10.5	3.06E-31
GO:0000323	lytic vacuole	153	1.0	40	6.5	8.65E-29
GO:0005764	lysosome	153	1.0	40	6.5	8.65E-29
GO:0005773	vacuole	173	1.2	41	6.6	3.18E-26
GO:0019882	antigen processing and presentation	43	0.3	28	4.5	4.23E-18
GO:0048002	antigen processing and presentation of peptide antigen	28	0.2	23	3.7	3.31E-16
GO:0006952	defense response	353	2.4	51	8.2	6.81E-16
GO:0044444	cytoplasmic part	2791	18.7	196	31.7	1.28E-12
GO:0005737	cytoplasm	4861	32.5	295	47.7	5.58E-12
GO:0019884	antigen processing and presentation of exogenous antigen	22	0.1	16	2.6	2.34E-10
GO:0002478	antigen processing and presentation of exogenous peptide antigen	17	0.1	14	2.3	1.89E-09
GO:0042611	MHC protein complex	19	0.1	14	2.3	4.69E-09
GO:0006412	translation	385	2.6	44	7.1	1.60E-08
GO:0002474	antigen processing and presentation of peptide antigen via MHC class I	14	0.1	12	1.9	3.47E-08
GO:0019886	antigen processing and presentation of exogenous peptide antigen via MHC class II	15	0.1	12	1.9	4.97E-08
GO:0002495	antigen processing and presentation of peptide antigen via MHC class II	15	0.1	12	1.9	4.97E-08
GO:0003735	structural constituent of ribosome	143	1.0	23	3.7	7.41E-08
GO:0002504	antigen processing and presentation of peptide or polysaccharide antigen via MHC class II	16	0.1	12	1.9	7.57E-08
GO:0002252	immune effector process	113	0.8	20	3.2	7.57E-08
GO:0006954	inflammatory response	178	1.2	26	4.2	1.05E-07
GO:0005840	ribosome	148	1.0	23	3.7	1.83E-07
GO:0030529	ribonucleoprotein complex	350	2.3	39	6.3	3.78E-07
GO:0009897	external side of plasma membrane	121	0.8	20	3.2	4.47E-07
GO:0016064	immunoglobulin mediated immune response	55	0.4	17	2.7	5.25E-07
GO:0019724	B cell mediated immunity	56	0.4	17	2.7	6.41E-07
GO:0005829	cytosol	316	2.1	36	5.8	6.81E-07
GO:0009611	response to wounding	252	1.7	31	5.0	7.65E-07
GO:0002449	lymphocyte mediated immunity	75	0.5	19	3.1	8.81E-07
GO:0002443	leukocyte mediated immunity	81	0.5	19	3.1	2.52E-06

(FDR < 0.05)

Immunohistochemical analysis of macrophages/microglia and iNOS.
Immunohistochemistry was performed with antibodies directed against ionized calcium-binding adaptor molecule 1 (Iba1; Wako, Tokyo, Japan; diluted 1 : 2000) or inducible nitric oxide synthase (iNOS; Abcam, Cambridge, MA, USA; diluted 1 : 200) as the primary antibody and a secondary antibody conjugated with horseradish-peroxidase-labeled polymer (EnVision+ kit, DAKO, Copenhagen, Denmark). To immunostain for Iba1 and iNOS, deparaffinized sections were subjected to heat treatment in Tris–EDTA buffer (pH 9) and 10 mM citrate buffer (pH 6), respectively. Endogenous peroxidase activity was blocked by incubation with 3% H_2O_2 for 5 min at room temperature. The tissue sections were then incubated in goat serum for 30 min at room temperature to prevent nonspecific reactions. The sections were exposed to each primary antibody at 4°C overnight and then incubated with the secondary antibody for 40 min at 37°C. The signals were detected with diaminobenzidine (ImmPACT DAB®, Vector Laboratories Inc., Burlingame, CA, USA), followed by counterstaining with Mayer's hematoxylin.

DNA extraction and quantitative PCR for the detection of *N. caninum* DNA. To prepare DNA, the brain of each *N. caninum*-infected mouse was thawed in 10 times its volume of DNA extraction buffer (0.1 M Tris–HCl [pH 9.0], 1% SDS, 0.1 M NaCl, 1 mM EDTA) with 100 μg/mL proteinase K at 55°C. DNA was extracted with a commercial kit (DNeasy Blood & Tissue Kit; Qiagen, Hilden, Germany) with a standard protocol recommended by the manufacturer. In addition to eight areas of brain (olfactory system, frontal lobe, caudate putamen, hippocampus, hypothalamus, amygdala, periaqueductal gray, and cerebellum), we estimate the parasite load in medulla oblongata because relatively severe histopathological changes were observed in the area. To evaluate the parasite load in the medulla oblongata, we used the DNA extracted from paraffin-embedded tissue sections from the 17 mice used for the pathological analysis. The sections contained the medulla oblongata and cerebellum because we could not remove the cerebellum from the samples. DNA was extracted from the paraffin-embedded tissues with a commercial kit (QIAamp® DNA FFPE Tissue Kit; Qiagen). The parasite DNA was amplified as described previously[41].

Briefly, we used the SYBR Green PCR Core Kit (PE Applied Biosystems, Foster City, CA, USA) and primers complementary to the Nc5 gene of *N. caninum*: the forward primer spanning nucleotides 248–257 (5′-ACT GGA GGC ACG CTG AAC AC-3′) and the reverse primer spanning nucleotides 303–323 (5′-AAC AAT GCT TCG CAA GAG GAA-3′). Amplification, data acquisition, and data analysis were carried out in the ABI Prism 7900HT Sequence Detection System (Applied Biosystems), and the calculated cycle threshold values (Ct) were exported to Microsoft Excel for analysis as described previously[11]. The limit of detection was 0.1 parasites in 50 ng of tissue DNA.

Transcriptome sequencing. Transcriptome sequencing was conducted as described previously[11]. Briefly, samples obtained from eight mice underwent poly-A selection with 1 μg of total RNA. Sequencing libraries were constructed with the RNA Sample Prep Kit (Illumina, San Diego, CA, USA); 36-bp single-end sequencing was performed using the Illumina Genome Analyzer IIx (Illumina) with the TruSeq SBS Kit v5-GA (36 cycle) (Illumina), according to the manufacturer's instructions. All treatment and following analyses associated with transcriptome sequencing were done individually.

Aligning sequence tags to the mouse genome and RefSeq. Aligning sequence tags was conducted as described previously[11]. Briefly, the raw sequence reads were mapped to the mouse genome (mm10) using TopHat (ver. 1.3.3 doi:10.1093/bioinformatics/btp120) allowing two mismatches and gtf data (Mus_musculus.GRCm38.69). The normalized transcription profiles were estimated based on the mapping results using cufflinks (doi:10.1038/nbt.1621). The number of fragments/kb of transcript/million fragments mapped (FPKM) was converted from the raw read counts for each transcript. The MGI ID and gene ontology (GO) were obtained from the Mouse Genome Informatics database[42], and then integrated into the estimated expression profiles, together with the gene biotypes extracted from the gtf data.

Table 4 | Thirty most overrepresented GO terms for the genes that correlated negatively with the parasites load

Accession	GO term	Reference gene		Genes negatively correlated with parasite number		FDR
		# Genes	%	# Genes	%	
GO:0042995	cell projection	333	2.2	23	8.9	6.75E-08
GO:0043005	neuron projection	108	0.7	16	6.2	1.27E-06
GO:0005886	plasma membrane	1476	9.9	56	21.7	2.07E-06
GO:0051179	localization	2430	16.3	78	30.2	7.01E-06
GO:0016192	vesicle-mediated transport	375	2.5	21	8.1	9.05E-05
GO:0006810	transport	2099	14.1	65	25.2	6.52E-04
GO:0016125	sterol metabolic process	67	0.4	10	3.9	6.52E-04
GO:0051234	establishment of localization	2152	14.4	66	25.6	6.52E-04
GO:0008202	steroid metabolic process	130	0.9	13	5.0	6.52E-04
GO:0048667	neuron morphogenesis during differentiation	153	1.0	14	5.4	6.52E-04
GO:0048812	neurite morphogenesis	153	1.0	14	5.4	6.52E-04
GO:0016126	sterol biosynthetic process	26	0.2	7	2.7	6.52E-04
GO:0050808	synapse organization and biogenesis	39	0.3	8	3.1	6.52E-04
GO:0007268	synaptic transmission	179	1.2	15	5.8	6.52E-04
GO:0000267	cell fraction	422	2.8	21	8.1	6.80E-04
GO:0019226	transmission of nerve impulse	211	1.4	16	6.2	8.53E-04
GO:0030424	axon	58	0.4	9	3.5	8.72E-04
GO:0016020	membrane	6123	41.0	144	55.8	9.91E-04
GO:0008324	cation transmembrane transporter activity	435	2.9	21	8.1	1.08E-03
GO:0008203	cholesterol metabolic process	61	0.4	9	3.5	1.08E-03
GO:0007409	axonogenesis	146	1.0	13	5.0	1.10E-03
GO:0006836	neurotransmitter transport	46	0.3	8	3.1	1.10E-03
GO:0000904	cellular morphogenesis during differentiation	172	1.2	14	5.4	1.10E-03
GO:0030030	cell projection organization and biogenesis	252	1.7	17	6.6	1.10E-03
GO:0048858	cell projection morphogeneisis	252	1.7	17	6.6	1.10E-03
GO:0032990	cell part morphogenesis	252	1.7	17	6.6	1.10E-03
GO:0006695	cholesterol biosynthetic process	20	0.1	6	2.3	1.16E-03
GO:0031175	neurite development	183	1.2	14	5.4	1.99E-03
GO:0048699	generation of neuron	299	2.0	16	6.2	2.12E-03
GO:0015075	ion transmembrane transporter activity	595	4.0	25	9.7	2.46E-03

(FDR < 0.05)

Identification of differentially expressed genes. Aligning sequence tags was conducted as described previously[11]. Briefly, differentially expressed genes were identified with the DESeq package in the R software[43], using a two-fold change (log2 fold-change >1 or <−1) and a 5% false discovery rate (FDR) cut-off for the thresholds. The expression intensity values were analyzed with an MA plot-based method after data normalization and the calculation of FDR.

Gene ontology (GO) analysis. The function of individual genes can be analyzed with GOstat (http://gostat.wehi.edu.au/), as described previously[11]. Using GOstat, we identified GO terms statistically overrepresented in the selected genes compared with the reference genes (all genes; 14938 genes). The statistical analysis was performed with a Benjamini correction, which controls FDR[44]. FDRs < 0.05 were considered statistically significant.

Correlation between gene expression levels and parasite numbers. The correlation coefficients for the FPKM values and the numbers of parasites in the mouse brain were calculated using Pearson's correlation coefficient, as previously described[11]. The range of correlation coefficients for positive correlations was 0.7 to 1.0, and the no-correlation range was −0.7 to 0.7, whereas the range for negative correlation was −0.7 to −1. We analyzed genes that correlated positively or negatively with the number of parasites in the mouse brain using GOstat.

Quantitative reverse-transcription-PCR (qRT-PCR). Steady state mRNA expressions of the genes that upregulated by *N. caninum* infection and downregulated in symptomatic mice infected with the parasites were measured by qRT-PCR. Total RNA was extracted using TRI Reagent (Sigma, St Louis, MO, USA), from the left halves of brains. Reverse transcription was performed using Superscript III™ Reverse

Table 5 | Genes significantly altered in brain samples from mice exhibiting clinical signs of neosporosis

Gene symbol	Description	Average of FPMK		FPKM Fold change	FDR
		No signs (n = 2)	Clinical signs (n = 2)		
Hoxb5	homeobox B5	1.09	0.09	0.08	7.33.E-04
Slc6a4	solute carrier family 6 (neurotransmitter transporter, serotonin), member 4	2.94	0.38	0.13	3.04.E-09
BC037034	cDNA sequence BC037034	10.04	1.44	0.14	9.05.E-03
Tph2	tryptophan hydroxylase 2	4.03	0.88	0.22	6.85.E-06
Slc6a5	solute carrier family 6 (neurotransmitter transporter, glycine), member 5	4.15	0.95	0.23	3.84.E-06
Mab21l2	mab-21-like 2 (C. elegans)	3.26	1.08	0.33	2.41.E-02
Fos	FBJ osteosarcoma oncogene	33.97	12.06	0.36	5.30.E-03
Ldlr	low density lipoprotein receptor	7.42	2.89	0.39	9.05.E-03

(>two-fold change and FDR < 0.05)

Transcriptase (Invitrogen, Life Technologies, Carlsbad, CA, USA), according to the manufacturer's instruction. Real-time PCR was performed using an Applied Biosystems Prism 7700 Sequence Detection System with SYBR Green master mix (AB Applied Biosystems, Life Technologies, Carlsbad, CA, USA). The fold change C_t method was used, where C_t is the threshold concentration (User Bulletin no. 2; Perkin-Elmer, Boston, MA, USA). Glyceraldehyde-3-phosphate dehydrogenase (GAPDH) mRNA was used as a control. Specific primer sequences were shown in Table S5.

1. Tranas, J., Heinzen, R. A., Weiss, L. M. & McAllister, M. M. Serological evidence of human infection with the protozoan *Neospora caninum*. *Clin. Diagn. Lab. Immunol.* **6**, 765–767 (1999).
2. Ho, M. S. *et al*. Detection of *Neospora* from tissues of experimentally infected rhesus macaques by PCR and specific DNA probe hybridization. *J. Clin. Microbiol.* **35**, 1740–1745 (1997).
3. Reichel, M. P., Ellis, J. T. & Dubey, J. P. Neosporosis and hammondiosis in dogs. *J Small Anim Pract.* **48**, 308–312 (2007).
4. Dubey, J. P., Schares, G. & Ortega-Mora, L. M. Epidemiology and control of neosporosis and *Neospora caninum*. *Clin. Microbiol. Rev.* **20**, 323–367 (2007).
5. Dubey, J. P. Review of *Neospora caninum* and neosporosis in animals. *Korean J. Parasitol.* **41**, 1–16 (2003).
6. Dubey, J. P. & Schares, G. Neosporosis in animals–the last five years. *Vet. Parasitol.* **180**, 90–108 (2011).
7. Buxton, D., McAllister, M. M. & Dubey, J. P. The comparative pathogenesis of neosporosis. *Trends Parasitol.* **18**, 546–52 (2002).
8. Cantile, C. & Arispici, M. Necrotizing cerebellitis due to *Neospora caninum* infection in an old dog. *J Vet Med A Physiol Pathol Clin Med.* **49**, 47–50 (2002).
9. Barber, J. S., Payne-Johnson, C. E. & Trees, A. J. Distribution of *Neospora caninum* within the central nervous system and other tissues of six dogs with clinical neosporosis. *J Small Anim Pract.* **37**, 568–574 (1996).
10. McConkey, G. A., Martin, H. L., Bristow, G. C. & Webster, J. P. *Toxoplasma gondii* infection and behaviour - location, location, location? *J. Exp. Biol.* **216**, 113–119 (2013).
11. Tanaka, S. *et al*. Transcriptome analysis of mouse brain infected with *Toxoplasma gondii*. *Infect. Immun.* **81**, 3609–3619 (2013).
12. Long, M. T., Baszler, T. V. & Mathison, B. A. Comparison of intracerebral parasite load, lesion development, and systemic cytokines in mouse strains infected with *Neospora caninum*. *J. Parasitol.* **84**, 316–320 (1998).
13. Reichel, M. P. & Ellis, J. T. *Neospora caninum*–how close are we to development of an efficacious vaccine that prevents abortion in cattle? *Int. J. Parasitol.* **39**, 1173–1187 (2009).
14. Garosi, L. *et al*. Necrotizing cerebellitis and cerebellar atrophy caused by *Neospora caninum* infection: magnetic resonance imaging and clinicopathologic findings in seven dogs. *J. Vet. Intern. Med.* **24**, 571–578 (2010).
15. Lorenzo, V., Pumarola, M. & Sisó, S. Neosporosis with cerebellar involvement in an adult dog. *J Small Anim Pract.* **43**, 76–79 (2002).
16. Baszler, T. V., Long, M. T., McElwain, T. F. & Mathison, B. A. Interferon-gamma and interleukin-12 mediate protection to acute *Neospora caninum* infection in BALB/c mice. *Int. J. Parasitol.* **29**, 1635–1646 (1999).
17. Vázquez-Boland, J. *et al*. *Listeria* pathogenesis and molecular virulence determinants. *Clin Microbiol Rev.* **14**, 584–640 (2001).
18. Join-Lambert, O. F. *et al*. *Listeria monocytogenes*-infected bone marrow myeloid cells promote bacterial invasion of the central nervous system. *Cell Microbiol.* **7**, 167–180 (2005).
19. Bal-Price, A. & Brown, G. C. Inflammatory neurodegeneration mediated by nitric oxide from activated glia-inhibiting neuronal respiration, causing glutamate release and excitotoxicity. *J. Neurosci.* **21**, 6480–6491 (2001).
20. Brown, G. C. & Neher, J. J. Inflammatory neurodegeneration and mechanisms of microglial killing of neurons. *Mol. Neurobiol.* **41**, 242–247 (2010).
21. MacMicking, J. D. IFN-inducible GTPases and immunity to intracellular pathogens. *Trends Immunol.* **25**, 601–609 (2004).
22. Martens, S. *et al*. Disruption of *Toxoplasma gondii* parasitophorous vacuoles by the mouse p47-resistance GTPases. *PLoS Pathog.* **1**, e24 (2005).
23. Zhao, Y. O., Khaminets, A., Hunn, J. P. & Howard, J. C. Disruption of the *Toxoplasma gondii* parasitophorous vacuole by IFNgamma-inducible immunity-related GTPases (IRG proteins) triggers necrotic cell death. *PLoS Pathog.* **5**, e1000288 (2009).
24. Reid, A. J. *et al*. Comparative genomics of the apicomplexan parasites *Toxoplasma gondii* and *Neospora caninum*: Coccidia differing in host range and transmission strategy. *PLoS Pathog.* **8**, e1002567 (2012).
25. Wen, X. *et al*. Predominant interferon-γ-mediated expression of CXCL9, CXCL10, and CCL5 proteins in the brain during chronic infection with *Toxoplasma gondii* in BALB/c mice resistant to development of toxoplasmic encephalitis. *J. Interferon Cytokine Res.* **30**, 653–660 (2010).
26. Nishikawa, Y. *et al*. In the absence of endogenous gamma interferon, mice acutely infected with *Neospora caninum* succumb to a lethal immune response characterized by inactivation of peritoneal macrophages. *Clin. Diagn. Lab. Immunol.* **8**, 811–816 (2001).
27. Kawai, T. *et al*. Selective diapedesis of Th1 cells induced by endothelial cell RANTES. *J. Immunol.* **163**, 3269–3278 (1999).
28. Dénes, A., Humphreys, N., Lane, T. E., Grencis, R. & Rothwell, N. Chronic systemic infection exacerbates ischemic brain damage via a CCL5 (regulated on activation, normal T-cell expressed and secreted)-mediated proinflammatory response in mice. *J. Neurosci.* **3**, 10086–10095 (2010).
29. Louboutin, J. P., Chekmasova, A., Marusich, E., Agrawal, L. & Strayer, D. S. Role of CCR5 and its ligands in the control of vascular inflammation and leukocyte recruitment required for acute excitotoxic seizure induction and neural damage. *FASEB J.* **25**, 737–753 (2011).
30. Villalba, M. *et al*. Herpes simplex virus type 1 induces simultaneous activation of Toll-like receptors 2 and 4 and expression of the endogenous ligand serum amyloid A in astrocytes. *Med. Microbiol. Immunol.* **201**, 371–379 (2012).
31. Jang, S. Y. *et al*. Local production of serum amyloid a is implicated in the induction of macrophage chemoattractants in Schwann cells during wallerian degeneration of peripheral nerves. *Glia* **60**, 1619–1628 (2012).
32. Kwon, H. S. *et al*. Myocilin mediates myelination in the peripheral nervous system through ErbB2/3 signaling. *J Biol Chem.* **288**, 26357–26371 (2013).
33. Israelsson, C. *et al*. Closed head injury in a mouse model results in molecular changes indicating inflammatory responses. *J Neurotrauma.* **26**, 1307–1314 (2009).
34. Gupta, N. & Rao, P. V. Transcriptomic profile of host response in Japanese encephalitis virus infection. *Virol J.* **8**, 92 (2011).
35. Pfrieger, F. W. & Ungerer, N. Cholesterol metabolism in neurons and astrocytes. *Prog. Lipid Res.* **50**, 357–371 (2011).
36. Guo, J., Chi, S., Xu, H., Jin, G. & Qi, Z. Effects of cholesterol levels on the excitability of rat hippocampal neurons. *Mol. Membr. Biol.* **25**, 216–223 (2008).
37. Chinoy, M. R. *et al*. Growth factors and dexamethasone regulate Hoxb5 protein in cultured murine fetal lungs. *Am J Physiol.* **274**, L610–20 (1998).
38. Gomeza, J. *et al*. Deletion of the mouse glycine transporter 2 results in a hyperekplexia phenotype and postnatal lethality. *Neuron.* **40**, 797–806 (2003).
39. Walther, D. J. & Bader, M. A unique central tryptophan hydroxylase isoform. *Biochem. Pharmacol.* **66**, 1673–1680 (2003).
40. Dubey, J. P., Carpenter, J. L., Speer, C. A., Topper, M. J. & Uggla, A. Newly recognized fatal protozoan disease of dogs. *J. Am. Vet. Med. Assoc.* **192**, 1269–1285 (1988).
41. Nishimura, M. *et al*. Oligomannose-coated liposome-entrapped dense granule protein 7 induces protective immune response to *Neospora caninum* in cattle. *Vaccine.* **31**, 3528–3535 (2013).
42. Eppig, J. T., Blake, J. A., Bult, C. J., Kadin, J. A. & Richardson, J. E. The Mouse Genome Database (MGD): comprehensive resource for genetics and genomics of the laboratory mouse. *Nucleic Acids Res.* **40**, D881–D886 (2012).
43. Anders, S. & Huber, W. Differential expression analysis for sequence count data. *Genome Biol.* **11**, R106 (2010).
44. Benjamini, Y. & Hochberg, Y. Controlling the false discovery rate – a practical and powerful approach to multiple testing. *J. Roy. Statist. Soc. Ser. B.* **57**, 289–300 (1995).

Author contributions

Y.N. designed research. M.N., S.T., F.I. and Y.M. performed experiments. M.N. and H.F. analyzed tissues histopathologically and with immunohistochemistry. S.T., J.Y. and Y.S. conducted transcriptome analysis. Y.N., M.N. and S.T. discussed results and drafted the manuscript. All authors have primary responsibility for final content. All authors read and approved the manuscript.

Additional information

Supplementary information accompanies this paper at http://www.nature.com/scientificreports

Competing financial interests: The authors declare no competing financial interests.

How to cite this article: Nishimura, M. *et al*. Transcriptome and Histopathological Changes in Mouse Brain Infected with *Neospora caninum*. *Sci. Rep.* **5**, 7936; DOI:10.1038/srep07936 (2015).